Annuaire de l'Université "St. Kliment Ohridski", Faculté de Physique, 98, 2005

OPTICAL PROPERTIES AND INTERFACE QUALITY OF GaAs QUANTUM WELLS EMBEDDED IN SHORT-PERIOD AlAs/GaAs SUPERLATTICES

VESSELIN DONCHEV, KRASSIMIRA GERMANOVA*, NIKOLAY SHTINKOV**

Department of Condensed Matter Physics
**Department of Solid State Physics and Microelectronics*
***Department of Engineering Physics, Polytechnic School of Montreal, Canada*

Веселин Дончев, Красимира Германова, Николай Щинков. ОПТИЧНИ СВОЙСТВА И КАЧЕСТВО НА ИНТЕРФЕЙСИТЕ В КВАНТОВИ ЯМИ ОТ GaAs, ВЛОЖЕНИ В СВРЪХРЕШЕТКИ ОТ AlAs/GaAs

Представено е детайлно оптично изследване на квантови ями от GaAs, вложени в свръхрешетки от AlAs/GaAs. Проведени са фотолуминесцентни (ФЛ) измервания в набор от образци с различна геометрия и температура на израстване. От анализа на профила на ФЛ линии е получена количествена оценка за относителните приноси на свободни екситони и свободни токоносители в процеса на излъчвателна рекомбинация. Намерено е, че приносът на свободните токоносители нараства с температурата, но свободните екситони доминират излъчвателната рекомбинация в целия интервал от хелиеви до стайни температури. Енергиите на оптични преходи, определени от анализа на профила на ФЛ линии, са сравнени със съответните енергии, пресметнати в рамките на модел, основан на приближението на обвиващите функции, който включва нерезки интерфейси. В този модел концентрационният профил в направление, перпендикулярно на интерфейса, се представя като резултат от взаимна дифузия на материалните компоненти (Al и Ga), при което дифузионната дължина е параметър, определящ размиването на интерфейса. От сравнението е оценена степента на размиване на интерфейсите в различните изследвани образци. Дискутирано е влиянието на условията за получаване върху качеството на интерфейсите на структурите.

Vesselin Donchev, Krassimira Germanova, Nikolay Shtinkov. OPTICAL PROPERTIES AND INTERFACE QUALITY OF GaAs QUANTUM WELLS EMBEDDED IN SHORT-PERIOD AlAs/GaAs SUPERLATTICES

A detailed optical study of GaAs quantum wells embedded in AlAs/GaAs superlattices is presented. Photoluminescence (PL) measurements are carried out on a number of samples with different geometry and growth temperature. The line-shape analysis of the PL peaks provides a quantitative estimate of the relative contributions of free excitons and free carriers to the radiative recombination process. It is found that the contribution of free carriers increases with the temperature, but free excitons dominate the radiative recombination in whole the range from helium up to room temperature. The optical transitions energies found from the PL line-shape analysis are compared with the corresponding energies calculated in frames of an envelope function approximation based model, which incorporates graded interfaces. In this model, the concentration profile across the interfaces is represented as a result of material interdiffusion, the diffusion length being a parameter, determining the degree of the interface broadening. The comparison has allowed estimating the interface broadening in the different investigated nanostructures. The influence of the growth conditions on the interface quality is discussed.

Keywords: AlAs/GaAs superlattices, embedded quantum wells, photoluminescence spectra, line-shape analysis, interface grading, envelope function approximation, excitons

PACS numbers: 78.67.De, 78.67.Pt, 78.55.–m, 73.21.Fg

1. INTRODUCTION

Currently an increasing attention has been paid to the investigation of short-period AlAs/GaAs superlattices (SLs) containing embedded GaAs quantum wells (QWs). It has been shown that they have unique basic properties and allow fabrication of advanced device structures for optoelectronics, photonics, optical communications, etc. [1–9].

The photoluminescence (PL) measurements have been proved to be a valuable tool to study the electronic states and optical properties of QWs. In order to better understand the measured PL spectra, however further efforts are needed for improving and extending the theoretical analysis of the PL line-shapes. For example, the dominant recombination mechanism and the momentum conservation in the radiative recombination process in GaAs/AlGaAs single and multiple QWs remains an open question. Some authors have found that in a wide temperature range (2–300 K) free exitons dominate the radiative recombination [10–12], while others claim that free carrier recombination is the main radiative process at 300 K [13].

The effect of interface roughness on the electronic states and PL properties of different nanostructures is another problem of a prime importance in their characterisation. It is known that the real interfaces are rather graded than abrupt due to the intermixing of the material components [14, 15]. Different intermixing sources have been discussed in a variety of papers [14, 16–19]. The material intermixing at the interfaces can significantly affect the physical properties of the QWs and SLs and in particular the shape of their PL spectra [20–24].

Until now such effects have been discussed in a number of papers concerning mainly GaAs/AlGaAs single QWs or periodic multilayers [21,23,25]. In complicated nanostructures such as AlAs/GaAs SLs containing GaAs embedded quantum wells, the problems mentioned above have been less studied and understood. Their study and better understanding are very important especially at 300 K, which is the operating temperature of most optoelectronic devices.

In this paper we present a detailed PL study of molecular beam epitaxy (MBE) grown short-period AlAs/GaAs SLs with GaAs embedded wells (EWs). PL spectral measurements are performed at different temperatures from 2 to 300 K. A detailed analysis of the PL spectra is carried out using two approaches. The first one represents a PL line-shape analysis based on a simple statistical model, which takes into account both free exciton and free carrier recombination. The fit of the measured PL spectra performed by means of this model shows that free exitons play a predominant role in the radiative recombination up to room temperature. The thermal equilibrium between exitons and free carriers is well described by the mass action law. It is found also that the PL line-shape is affected by interface imperfections.

In the second approach, the optical transition energies are calculated by means of an envelope function approximation (EFA) based model, taking into account the exciton binding energies. The model incorporates a graded potential at the interfaces, which is represented by a diffusion potential, the diffusion length being a parameter, determining the degree of interface broadening. A good agreement between the calculated excitonic transition energies and those derived from the fits is found and this way an estimate of the interface broadening in the different investigated nanostructures is obtained. The influence of the growth conditions on the interface quality is discussed. Complicated PL structures connected with the SL are also observed in the PL spectra. Their qualitative discussion confirms the main conclusions of the graded potential model. Thus the analysis of complicated AlAs/GaAs nanoheterostructures is extended to real interfaces, which is essential for advanced device fabrication.

2. EXPERIMENTAL

The samples investigated are grown by MBE on (001) GaAs substrates in EPFL (Ecole Polytechnique Fédérale de Lausanne), Switzerland. They represent $(AlAs)_4/(GaAs)_8$ SLs with one or two EWs [4 and 8 are the number of monolayers (ML) of AlAs and GaAs, respectively (1 ML = 0.283 nm)]. Two types of samples have been studied. Type A samples are grown at 600°C and include an EW of 5 nm (18 ML) sandwiched between 26 and 20 periods of SL, the first SL being grown directly on the substrate. Type B samples are grown at different temperatures between 550 and 680°C. They contain two EWs—one of 12 nm (42 ML) and one of 5 nm (18 ML), the latter being above the former. There are 5, 24 and 20 periods of SL situated bellow the 12 nm EW, between the EWs and above the 5 nm EW, respectively. In this case a GaAs buffer layer of 400 nm is grown between the

substrate and the first SL. Both types of samples have a cap layer of $Al_x.Ga_{1-x}As$ ($x = 0.33$ is the mean Al content in the SL), which is thick 50 and 30 nm in samples A and B, respectively. The sample designs are schematically represented on Fig. 1.

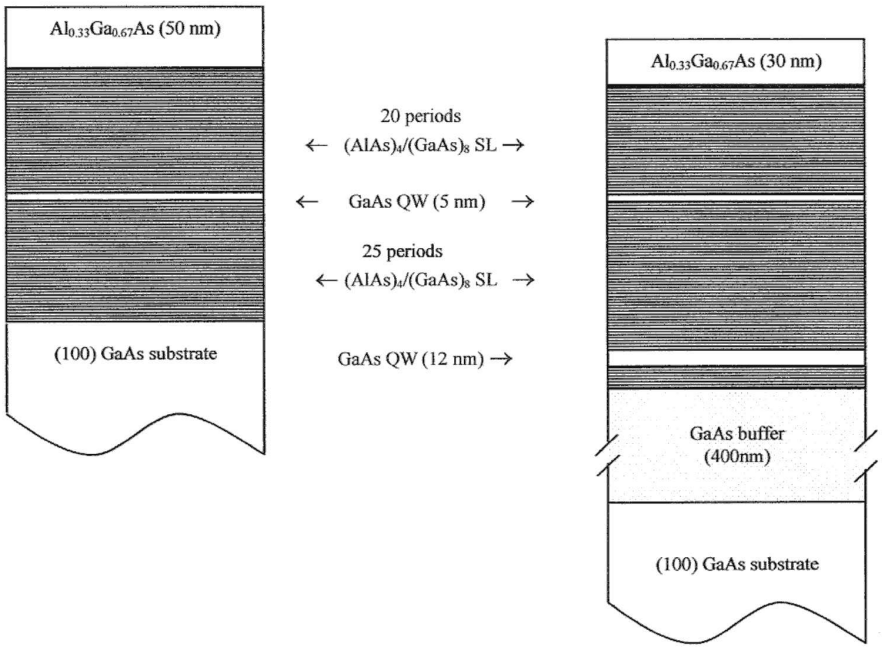

Fig. 1. Schematic representation of the experimental samples used in the studies

PL spectra are measured at different temperatures and excitation densities in the Laboratory of Electron and Phonon Properties of Solid State Materials and Structures (Faculty of Physics, Sofia University), in the Department of Physics and Measurement Technology (Linköping University, Sweden) and in the Institute of Opto- and Microelectronics, EPFL (Switzerland). Standard optical techniques for PL measurements are used. The basic characteristics of the set-ups and the experimental conditions are given in Table 1.

It is found that the PL spectra do not depend on the excitation wavelength used in the experiments. At low excitation densities the PL peak positions do not depend on the excitation power. That is, why in the description and the discussion below we give only the temperature of the measurements. The other conditions are given only if necessary.

Table 1. Experimental set-ups and conditions applied in the PL measurements

Series	1	2	3	4
T, K	2–300	2–300	300	77
Illumination	He–Ne laser	Ar laser	Ar laser	Semicond.laser
λ, nm	632.8	501	488	520
P, W/cm^2	1–34	4–400	300–3000	70
Monochro-mator	Double SPEX ($f = 0.85$ m)	Jobin Yvon ($f = 0.46$ m)	Double SPEX ($f = 0.85$ m)	Jobin Yvon ($f = 0.46$ m)
Detector	GaAs Photomultiplier	CCD–line detector	GaAs Photomultiplier	Si
Resolution	0.15 nm	0.025 nm	0.8 nm	1 nm
Location	Linkoeping University, Sofia University	Linkoeping University	Sofia University	EPFL, Switzerland

3. ANALYSIS OF THE PL SPECTRA

3.1. BASIC FEATURES OF THE PL SPECTRA

Typical PL spectra of samples type A and B are shown on Fig. 2. Sharp PL peaks related to electron–heavy hole transitions in the EWs are observed at low temperature. They are labelled P3 in samples A and P1 and P3 in samples B. The peaks broaden with increasing the temperature and small peaks or shoulders, P2 and P4, appear on their high-energy sides, corresponding to electron–light hole transitions. Since P1 and P2 are present only in the spectra of samples B, they are attributed to the 12 nm EW. Similarly P3 and P4 are ascribed to the EW of 5 nm.

The high-energy region of the 2K spectra reveals a sharp peak S2 and a wider low energy satellite S1, which has a shoulder in A samples (see Fig. 3). These peaks are ascribed to electron–heavy hole transitions in the SL (see below).

3.2. EXCITON BINDING ENERGIES

The knowledge of the exciton binding energies E_b is necessary for the comparison between the calculated and the experimental optical transition energies (see below). The precise calculation of E_b requires the use of complicated many-bands EFA models [26]. For a single GaAs/AlGaAs QW, they could be calculated by means of a simple interpolation formula proposed in [27]. In the case of EW, one can expect that the excitons will be more delocalised in the SL and therefore the exciton binding energies will be lower than for single QW. That is, why we use in

a first approximation the values of E_b calculated in [28] for a GaAs/AlAs/AlGaAs QW with double barrier. They are given in Table 2.

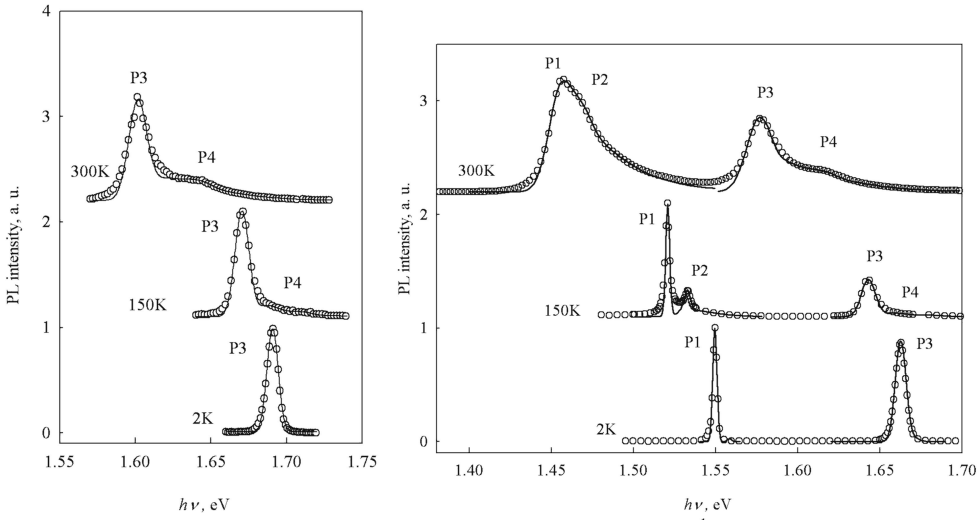

Fig. 2. PL spectra (circles) at different temperatures and fits of the PL peaks (lines) for samples type A (a) and B (b). The spectra at 150 K and 300 K are shifted upward for clarity

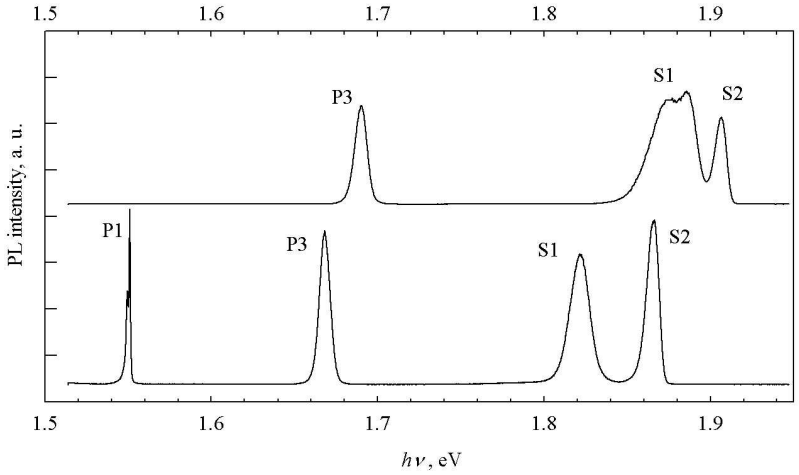

Fig. 3. PL spectra of samples type A (up) and B (down) measured at 2 K in a large spectral range. The spectrum of sample type A is shifted upward for clarity

Table 2. Exciton binding energies for heavy-hole (E_{bh}) and light-hole (E_{bl}) transitions

Embedded well (nm)	E_{bh} (meV)	E_{bl} (meV)
5	12	13.5
12	9	10.5

3.3. MAIN RADIATIVE RECOMBINATION MECHANISMS

The mechanisms of radiative recombination in complicated quantum heterostructures, such as SL with EWs are not systematically studied until now. However, this is a problem of prime importance, especially at room temperature, which is the operating temperature of most of the optical and optoelectronic devices based on the above-depicted structures. We have performed a detailed analysis of this problem using two approaches.

Excitation Density Dependence of the PL Intensity. The dependence of the integrated PL line intensity on the excitation density has a power form $I_{\mathrm{PL}} \sim I_{\mathrm{exc}}^{\alpha}$, where the value of the exponent α indicates the main recombination mechanism as follows: $\alpha = 1$ for free exciton recombination and $\alpha = 2$ for free carrier recombination [4,13]. We have applied this approach to analyse the P1 and P3 peaks at 2K and the same peaks with their shoulders (P1 + P2 and P2 + P4) at 300 K. The values of α obtained for different PL lines and different samples are in the range 1.06–1.22 at 2K and 1.25–1.67 at 300 K. These results show qualitatively that the recombination at low temperature (2 K) is excitonic. Moreover, free excitons dominate the recombination up to room temperature, where a contribution of free carriers is also present. This is confirmed quantitatively by the analysis in the next section.

Line Shape Analysis. In the second approach, a line-shape analysis of the PL peaks is performed. They are fitted using a simple statistical model, which takes into account both free exciton and free carrier recombination [4, 5, 10, 29]. Two Gaussians, multiplied by the corresponding statistical distributions describe the discrete HH and LH exciton lines. The free carrier recombination terms include a broadened step-like 2D density of states, multiplied by the free carrier statistical distribution in Boltzmann approximation and the 2D Sommerfeld factor, which takes into account the Coulomb interaction between electrons and holes. Thus, the emission intensity is a sum of the following terms:

$$I_{xi}(h\nu) = A_{xi} \exp\left[-\frac{(h\nu - E_{xi})^2}{2\sigma_{xi}^2}\right] \exp\left(-\frac{h\nu - E_{xi}}{kT}\right), \qquad (i = \mathrm{HH}, \mathrm{LH}) \qquad (1)$$

and

$$I_{ci}(h\nu) = A_{ci} \frac{1}{1+\exp\left(-\dfrac{h\nu - E_{ci}}{\sigma_{ci}}\right)} \exp\left(-\frac{h\nu - E_{ci}}{kT}\right) \times \frac{2}{1+\exp\left(-2\pi\sqrt{\dfrac{R_i}{|h\nu - E_{ci}|}}\right)} \qquad (i = \mathrm{HH}, \mathrm{LH}). \tag{2}$$

Here A_{xi}, E_{xi} and σ_{xi} (i = HH,LH) denote the amplitude, the energy and the broadening parameter of the heavy-hole (HH) and light-hole (LH) exciton lines; A_{ci}, E_{ci}, σ_{ci} are the amplitude, the energy and the broadening parameter of the electron-to-HH and electron-to-LH free–carrier recombination; and R_i is the effective Rydberg, i.e., the exciton binding energy E_{bi}.

Table 3. Temperature dependence of the ratio F/X of the contributions of free excitons (X) and free carriers (F) to the radiative recombination in samples A and B

T(K)	F/X		
	Type B		Type A
	12 nm EW	5 nm EW	5 nm EW
2	0	0	0
64	0.07	0.02	0.02
77	0.12	0.04	–
80	–	–	0.03
100	0.18	0.08	0.07
150	0.44	0.20	0.22
206	–	–	0.34
300	0.95	0.63	0.73

Fig. 2 shows that the theoretical fits (solid lines) describe satisfactorily the main features of the experimental peaks. Using the fit results, we investigate the temperature evolution of the relative contributions of free excitons (X) and free carriers (F) to the radiative recombination, estimated by integrating the corresponding terms in the fitting formulae. Table 3 represents the values of the ration F/X at different temperatures in two samples (type A and B). At 2 K the PL peaks P1 and P3 are described by single Gaussians, corresponding to HH exciton recombination. The LH exciton and the free carrier transitions are not present in the spectra. So, the radiative recombination at 2 K is purely excitonic

($F = 0$). With increasing the temperature, the free carrier contribution increases and so does the ratio F/X. Its values are larger for the wider EW in accordance with the smaller exciton binding energies in this case. At room temperature F is comparable to X, but free exciton recombination still prevails: F/X is in the range from 0.84 to 0.95 for the 12 nm EW, and from 0.63 to 0.82 for the 5 nm EW in different samples. These findings show that free exciton recombination is dominant in our samples at all the temperatures used.

The careful analysis of the theoretical and experimental curves displayed in Fig. 2 shows two interesting features:

i) The fits cannot reproduce satisfactorily the broadening of the high-energy side of the HH exciton peaks (P1 and P3). This broadening results from exciton recombination at low temperature without momentum conservation [11, 30], while in the model used a momentum conservation is assumed.

ii) The low-energy sides of the peaks are reproduced with minor accuracy, because the model does not take into account the recombination of excitons bound to potential fluctuations at the interfaces [30,31] due to interface imperfections.

These effects are an indication that in the investigated structures the interfaces are not perfect. This is confirmed also in the following section.

In spite of these effects the peak parameters can be quite well estimated in frames of the theoretical model used, as discussed in [30]. The following facts also confirm the correctness of the model:

i) The plots of $\mathrm{Ln}[F/(X * T)]$ versus $1/T$ corresponding to the P1–P2 and P3–P4 emission lines are linear (Fig. 4). Their slopes are in good agreement with the exciton binding energies used in the calculations. Thus, it is shown that the thermal equilibrium between excitons and free carriers is well described by the 2D mass action law [32].

ii) The exciton transition energies derived from the fits follow well the temperature behaviour of the GaAs gap down to 30 K (Fig. 5). The same energies determined directly from the PL peak positions have lower values, especially at low temperatures.

iii) The line broadening parameters increase with T (Fig. 6), due to exciton scattering by LO phonons. The broadening is greater for the P3 peaks, in accordance with the smaller EW width (Fig. 6).

At the end of this section we emphasize that the results obtained in frames of both approaches used show that the radiative recombination in QWs embedded in SLs is dominated by exciton recombination up to room temperature.

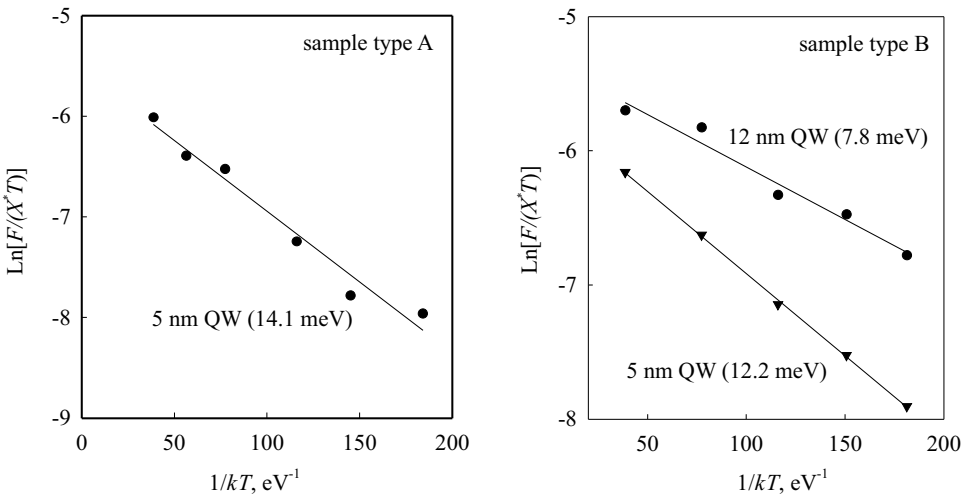

(*a*) (*b*)

Fig. 4. Arrhenius plots of F/XT for the peaks P1 and P3 from the QWs in samples type A (*a*) and B (*b*). The data obtained from the fit of the PL peaks at different temperatures are shown (points) together with a linear fir (lines). The slopes are indicated on the figure

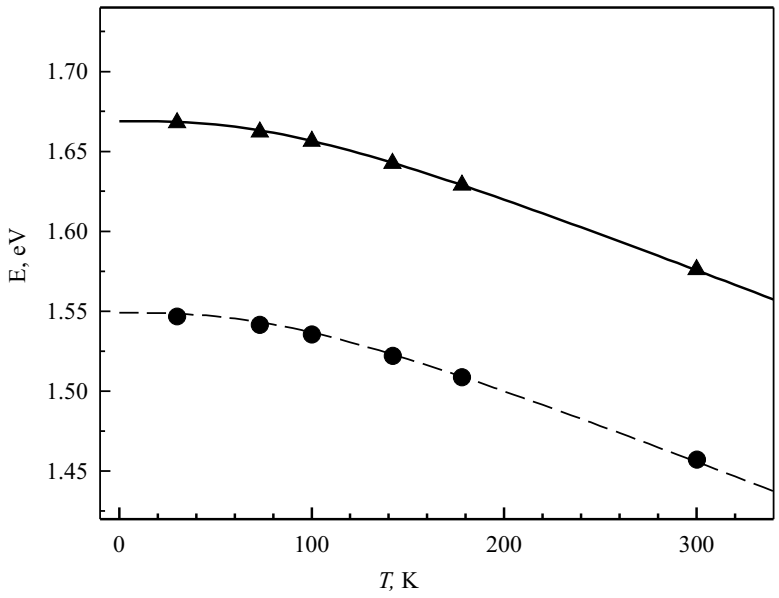

Fig. 5. Temperature dependence of the exciton transition energies, derived from the fits of the peaks P1 (•) and P3 (▲). The GaAs gap is also given (lines) shifted by 0.03 and 0.15 eV, respectively

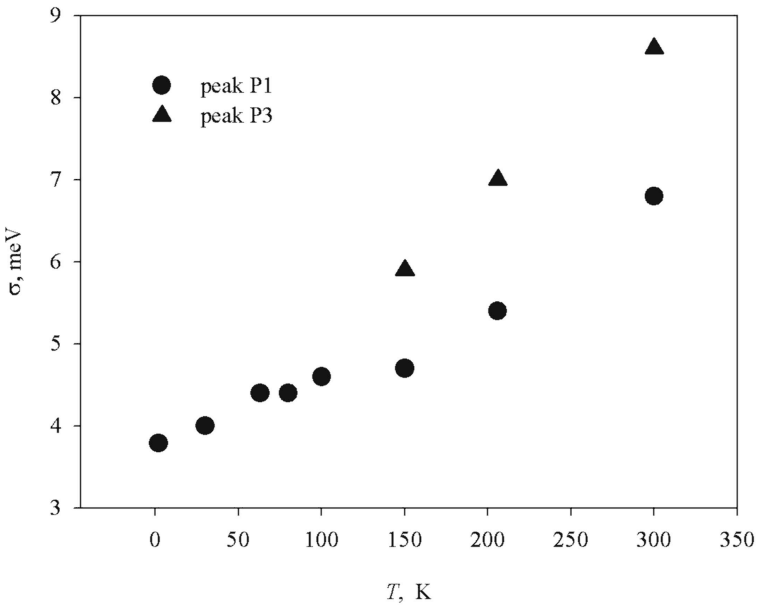

Fig. 6. Line broadening parameter as a function of the temperature for the peaks P1 (•) and P3 (▲)

3.4. DISCUSSION OF THE EXPERIMENTAL RESULTS IN FRAMES OF AN EFA MODEL, WHICH INCLUDES NON-ABRUPT INTERFACES

Non-abrupt interfaces and optical transition energies. In this section, a discussion of the interface grading effect on the PL spectral behaviour is given. The experimental optical transition energies, determined from the line-shape fits (Sect. 3.3.2), are compared with the ones calculated by the EFA taking into account the potential non-abruptness which is always present at real interfaces. In the interface model used in the calculations, the concentration profile across the interfaces is represented as a result of material interdiffusion, the diffusion length being a measure of the interface broadening. A more detailed description of this model is given in our previous papers [6–8].

Table 4 presents a comparison between the calculated energies of HH exciton transitions in both types of EWs and the experimental ones obtained in two samples—one of type A and one of type B. The exciton binding energies E_{bh} and the diffusion length L_D used in the calculations are also given. The energies calculated assuming abrupt interfaces ($L_{\mathrm{D}} = 0$) are lower than the experimental

ones. The difference is larger for the narrower well and is more pronounced in samples A than in samples B. The discrepancies decrease when the interface broadening is taken into account. The transition energies shift up with increasing L_D as shown in our previous works [8, 33]. Thus, a nearly perfect agreement between calculated and experimental values is achieved as follows (see Table 4). A broadened potential characterised by a diffusion length of 4.3 ML explains the energy position of the PL emission from the 5 nm EW in samples A. One and the same diffusion length of 3.4 ML accounts for the transition energies in both EWs in samples B. Note that the same value of L_{D} provokes different shifts in the transition energies in the two EWs. The shift is smaller in the larger EW, because in this well the wave functions of the first electron and hole states are less sensitive to potential grading at the interfaces.

Table 4. Comparison between calculated and experimental energies for heavy-hole exciton transitions two samples (type A and B)

Sample	Type A		Type B			
Embedded Well	5 nm		5 nm		12 nm	
L_{D}, ML	0	4.3	0	3.4	0	3.4
E_{bh}, meV	12	12	12	12	9	9
E_{EFA}, meV	1653	1696	1653	1680	1554	1558
$E_{\mathrm{EFA}} - E_{\mathrm{bh}}$, meV	1641	1684	1641	1668	1545	1549
$h\nu$, meV (peak)	1684 (P3)		1668 (P3)		1549 (P1)	

The larger value of $\mathrm{L_D}$, obtained for samples A indicates a larger interdiffusion and interfaces with lower quality in this case. This could be explained taking into account the following: i) The higher growth temperature of samples A leads to a larger Ga–Al interdiffusion during the growth process. This is discussed in more details in the next section; ii) As discussed in [14] the passage of defects through interfaces provokes a substantial intermixing. In our case, the diffusion of defects from the substrate to the EW is easier in samples A than in samples B, because in the former there is no buffer layer and the EW is closer to the substrate.

Thus, considering graded interfaces we are able to explain the energy positions of the PL peaks resulting from the EWs. Besides, the degree of interface broadening has been assessed from the comparison between calculated and experimental values.

Typical energy intervals between the peaks S1 and S2 in the high-energy region of the spectra are about 20 and 43 meV in samples A and B, respectively. A splitting of the SL exciton emission in two or more peaks has been observed by other authors and has been explained by unintentionally introduced interface imperfections and/or fluctuations in the thickness and in the potential of the SL layers [9,24]. All these peculiarities induce localised states both in space and in

energy. Thus, the SL mini–bands widen and split in subbands, which results in two or more PL peaks [9,24], as in our case. At low temperature these effects reduce considerably the vertical carrier transport to the EW. This accounts for the relatively high amplitude of the SL peaks compared to the ones of the EWs, as seen in Fig. 3.

We do not compare quantitatively the calculated and experimental energies of the SL transitions, because in the calculations we consider a SL with wells of equal width (except the central EW), and we use a potential averaged over the layer planes. Therefore our model does not account for the observed splitting of the PL emission from the SL (the two peaks S1 and S2). However the discussions carried out for the EWs apply qualitatively to the transitions in the SL. The larger degree of potential grading in samples A results in higher energies of the SL transitions, as seen in Fig. 3. The broad PL band S1 (which includes a shoulder) in the spectra of samples A also imply a larger intermixing in this case.

Our suggestion for the origin of the peaks S1 and S2 is confirmed also by data, obtaining via transmission electron microscopy (TEM). This is illustrated by the TEM-photo of a B type sample shown on Fig.7. The fluctuations of the widths of the SL layers are clearly seen.

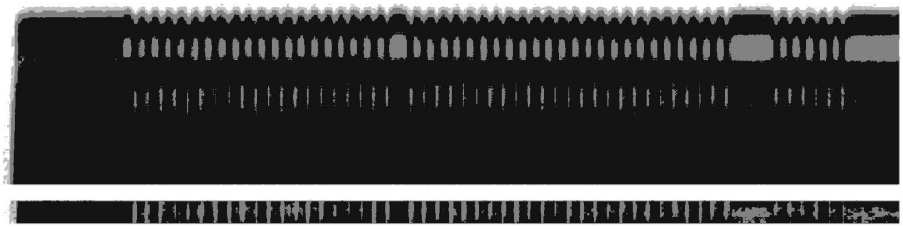

Fig. 7. Transmission electron microscopy photo of a sample type B

Interfaces quality of the investigated nanostructures. In this section, we compare the data (PL peak positions and calculated L_{D}) obtained in several samples grown at different substrate temperatures T_{s}. The results for B type samples are summarised in Table 5, where E_{cor} is the P3 peak energy increased by the exciton binding energy (12 meV, see Table 2) and the temperature correction (for the measurements at 77 K). The latter is necessary because of the different measurement temperatures. It is determined from the difference between the peak P3 positions at 2 K and 77 K in sample 3B and equals 3.9 meV. This value is lower than the shift of the GaAs gap with the temperature (6.7 meV for 77 K [34]) because of exciton localisation in potential fluctuations at the interfaces at low temperatures [12]. The value of L_{D} is determined comparing E_{cor} (P3) with the results of the EFA calculations. The following tendency is observed: increasing the growth temperature results in higher values of L_{D}, i.e. in lower quality of the interfaces. This finding is in agreement with the results from Ref. [6], where we

have performed a similar analysis, but using empirical tight-binding calculations. The quantitative analysis is not performed for the peak P1, because its sensitivity to the interface potential changes is very small. Nevertheless, its energy position follows the general trend of the peak P3, as can be seen from Table 5.

Table 5. PL peak positions and calculated values of L_D obtained in several samples type B, grown at different substrate temperatures T_s

Sample	T_{exp}, K	E(P1), eV	E(P3), eV	T_s, °C	E_{cor}(P3), eV	L_D, MC
1B	2	1.5491	1.6625	550	1.6745	3.0 (0)
2B	2	1.5493	1.6674	550	1.6794	3.3 (3)
3B	2	1.5392	1.6677	550	1.6797	3.3 (5)
4B	77	1.5382	1.6660	550	1.6819	3.4 (9)
5B	77	1.5398	1.6660	600	1.6819	3.4 (9)
6B	2	1.5511	1.6717	600	1.6837	3.6 (0)
7B	77	1.5426	1.6694	600	1.6853	3.6 (9)
8B	77	1.5436	1.6705	650	1.6864	3.7 (6)
9B	77	1.5436	1.6718	650	1.6877	3.8 (4)
10B	77	1.5465	1.6804	680	1.6963	4.3 (3)

Table 6. PL peak positions and calculated values of L_D obtained in several samples type A, grown at different substrate temperatures T_s

Sample	T_{exp}, K	E(P3), eV	T_s, °C	E_{corr}(P3), eV	L_D, MC
1A	2	1.6834	600	1.6954	4.2 (8)
2A	2	1.6844	600	1.6964	4.3 (3)
3A	2	1.6898	600	1.7018	4.6 (3)
4A	2	1.6893	600	1.7013	4.6 (0)

Table 6 presents the energies of the peaks P3 in A type samples together with the corresponding values of L_D calculated from them. The mean value of L_D at $T_s = 600$°C (4.46 ML) is considerably higher than that in B type samples grown at the same temperature (3.59 ML). This difference is seen also in Fig. 8, which displays the values of L_D obtained in each sample. As depicted in the previous section, the higher L_D values in A samples are related to the absence of a buffer layer in this case, which leads to lower quality of the interfaces.

The literature data for the AlAs/GaAs interfaces, obtained from the analysis

of high-resolution TEM measurements, give L_{D} values between 1 and 4 ML. The values found in our work for different samples are between 3.0 and 4.6 ML (see Tables 5 and 6), i.e., they are in good agreement with the literature data. In the same time, these values show a relatively large interface broadening in the investigated samples.

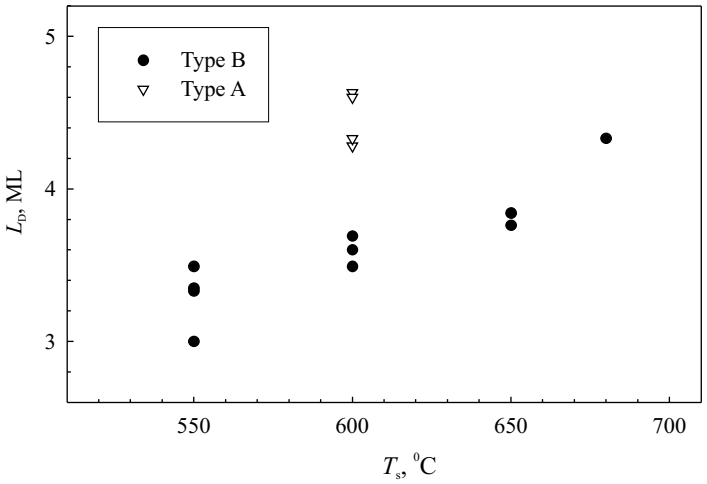

Fig. 8. Diffusion length values obtained for a number of samples type A($\bigtriangledown$) and B($\bullet$) grown at different substrate temperatures

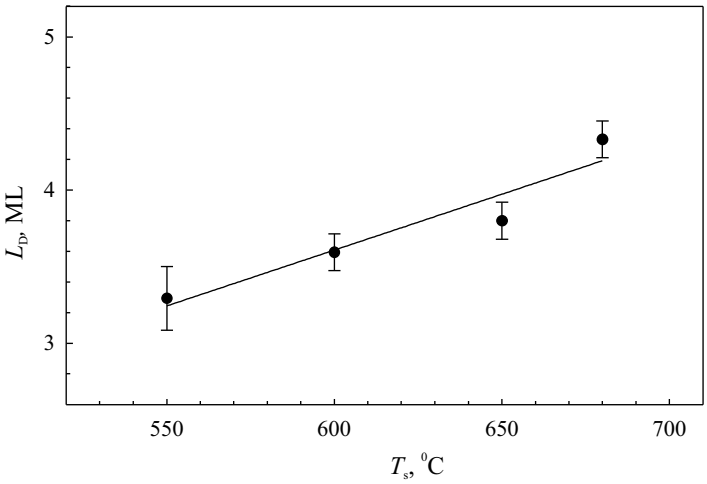

Fig. 9. The averaged value of the diffusion length obtained for different samples type B as a function of the substrate temperature. The line is only a guide for the eyes

Fig. 9 shows the values of L_D in B samples averaged at each of the four growth temperatures. The errors are estimated by calculating: i) the root mean squared deviation of the L_D values at the corresponding T_s and ii) the error in L_D corresponding to the 1 nm error in the PL peak position. The larger of these two values is given on Fig. 9. One can see that the averaged value of L_D increases with increasing the growth temperature. On the other hand the careful analysis of the data on Table 5 shows that L_D varies among different samples grown at the same substrate temperature. This implies that besides the interdiffusion other reasons could be responsible for the energy shift of the PL peaks with increasing T_s. Such a reason could be the interface roughness on an atomic scale, which is averaged over the layer planes in our model. Therefore, L_D must be considered as a parameter, which accounts for the averaged interface broadening in the growth direction of the structure.

4. CONCLUSION

GaAs quantum wells embedded in short-period AlAs/GaAs SL are studied by PL measurements at different temperatures using a number of samples with different geometry and growth temperature. The observed PL peaks have been identified as the HH and LH exciton transitions in the EWs and the SL. A detailed analysis of the PL line shapes is performed for the EW transitions, using a simple statistical model. As a result a quantitative estimate of the relative contributions of free excitons and free carriers to the radiative recombination in a wide temperature range (2 to 300 K) is obtained. It is found that free excitons recombination dominates the PL emission up to room temperature. This is confirmed also by the analysis of the excitation density dependence of the integrated PL intensity. The temperature behaviour of the PL peak energies and PL peaks broadening parameters follows the expected trends. Some discrepancies between the experimental and theoretical PL line-shapes are attributed to localised excitons, which indicate the presence of interface imperfections.

A very good agreement is obtained from the comparison between the exciton transition energies in the EWs determined from the fits and the corresponding energies calculated in frames of an EFA based model, which takes into account the interface grading due to material interdiffusion. The comparison has provided an estimate of the degree of interface broadening in the samples used. It is found that the interface broadening increases with increasing the growth temperature. On the other hand a buffer layer between the substrate and the SL improves the interface quality. The applied approach extends the analysis of complicated GaAs/AlGaAs heterostructures towards real interfaces, allowing a better description of their PL properties. It can also be used in the evaluation of various heterostructures with a larger degree of interface grading (obtained, e.g., by sample annealing) in order to exploit their new properties attractive for device fabrication.

Acknowledgements: Financial support from the Bulgarian National Science Fund and the Sofia University Research Fund is acknowledged. The authors are

grateful to D. Martin (EPFL) for supplying the samples and some PL and TEM data and to I. Ivanov (Linkoeping University) for performing PL measurements at hellium temperatures. Thanks are due to S. Vlaev for helpful discussions and to Tz. Ivanov, H. Brachkov, M. Angelov, and Tzv. Ivanov for technical help.

REFERENCES

1. Blood, P. In: Physics and Technology of Heterojunction Devices, Eds. D. V. Morgan, and R. H. Williams , Peter Perigrinus, London, 1991, 231.
2. Sakaki, H., M. Tsuchiya, J. Yshino. *Appl. Phys. Lett.* **47**, 1985, 295.
3. Kapon, E., G. Biasiol, D.M. Hwang, M. Walther, E. Colas. *Sol. St. Com.*, **40**, 1996, 815.
4. Donchev, V., Tzv. Ivanov, I. Ivanov, M. Angelov, K. Germanova. *Vacuum* **58**, 2000, 478.
5. Donchev, V., N.Shtinkov, K.Germanova, I.Ivanov, H.Brachkov, Tzv.Ivanov. *Mat. Sci. Engin. C* **15**, 2001, 75.
6. Shtinkov, N., V.Donchev, K.Germanova, S.Vlaev, I.Ivanov. *Vacuum* **58**, 2000, 561.
7. Donchev, V., K.Germanova, N.Shtinkov, I.Ivanov, S.Vlaev. *Thin Solid Films* **364**, 2000, 224.
8. Germanova, K., V. Donchev, N. Shtinkov, S. Vlaev. accepted in *Annual of University of Sofia, Faculty of Physics.*
9. Deveaud, B., J.Shah, T.C.Damen, B.Lambert, A.Chomette, A.Regreny. *IEEE J. Quantum Electronics* **24,** 1988, 1641.
10. Chen, Y., R. Cingolani, L. Andreani, F. Bassani, J. Massies. *Il Nuovo Cimento* **10D**, 1988, 847.
11. Christen, J., D. Bimberg. *Phys. Rev. B* **42**, 1990, 7213.
12. Fujiwara, K., N. Tsukada, T. Nakayama. *Appl. Phys. Lett.* **53**, 1988, 675.
13. Fouquet, J. E., A. E. Siegman. *Appl. Phys. Lett.* **46**, 280, 1984..
14. Ourmazd, A., M. Scheffler, M. Heinemann, J-L. Rouviere. *Mater.Res.Bulletin* **27**, 1992, 24.
15. Ourmazd, A., D.W.Taylor, J.Cunningham, C.W. Tu. *Phys. Rev. Lett.*, **62,** 1989, 933.
16. Jusserand, B., F. Mollot. *Appl. Phys. Lett.* **61**, 1992, 423.
17. Spencer, G.S., J. Menendez, L. N. Pfeiffer, K. W. West, *Phys. Rev. B* **52**, 1995, 8205.
18. Koiller, B., A. S. Martins, H. Chacham. *Appl.Phys.Lett.*, **69**, 1996, 2423.
19. Rouviere, J.-L., Y. Kim, J. Cunningham, J. A. Rentchler, A. Bourret, A.Ourmazd, *Phys. Rev. Lett.* **68**,1992, 2798.
20. Herman, M.A., D. Bimberg, J. Christen. *J.Appl.Phys.* **70**, R1, 1991.
21. Harrison, I. *Semicond. Sci. Technol.* **9** , 1994, 2053.
22. Warwick, C. A., R. F. Kopf. *Appl. Phys. Lett.*, **60,** 1992, 386.
23. Vlaev, S., D.A. Contreras-Solorio. *J. Appl. Phys.* **82**, 1997**,** 3853.
24. Pavesi, L., E.Tuncel, B.Zimmermann, F.K.Reinhart. *Phys.Rev. B* **39**, 1989, 7788.
25. Oh, Y.T., T.W. Kang, T.W. Kim. *J. Appl. Phys.* **78** , 1995, 3376.
26. Winkler, R. *Phys. Rev. B* **51**, 1995, 14395.
27. Oelgart, G., M. Proctor, D. Martin, F. Morier-Genaud, F. K. Reinhart, B. Orschel, L. C. Andreani, H. Rhan. *Phys. Rev. B* **49**, 1994, 10456.
28. Kupka, R.K, Y.Chen. *J. Appl. Phys.* **77**, 1995, 1990.
29. Colocci, M., M. Gurioli, A. Vinattieri. *J. Appl. Phys.* **68**, 1990, 2809.
30. Schnabel, R. F., R. Zimmermann, D. Bimberg, H. Nickel, R. Losch, W. Schlapp. *Phys. Rev. B* **46**, 1992, 9873.

31. de Oliveira, J. B. B., E. A. Meneses, E. C. F. da Silva. *Phys. Rev. B* **60**, 1999, 1519.
32. Chemla, D. S. *J. Luminesc.* **30**, 1985, 502.
33. Shtinkov, N., V. Donchev, K. Germanova, H. Kolev. *Semicond. Sci. Technol.* **15**, 2000, 946.
34. Data in Science and Technology. Semiconductors: Group IV Elements and III–V Compounds, Madelung, O. (Ed), Berlin: Springer, 1991.

Vesselin Donchev
St. Kliment Ohridsi University of Sofia
Faculty of Physics
Department of Condensed Matter Physics
5, James Bourchier, Blvd.
1164 Sofia, Bulgaria
E-mail: vtd@phys.uni-sofia.bg

Received December 2004